Dalton Transactions

ROYAL SOCIETY OF CHEMISTRY

COMMUNICATION

View Article Online
View Journal | View Issue

Cite this: *Dalton Trans.*, 2021, **50**, 1995

Received 26th November 2020,
Accepted 15th January 2021

DOI: 10.1039/d0dt04048g

rsc.li/dalton

MIL-101(Cr) with incorporated polypyridine zinc complexes for efficient degradation of a nerve agent simulant: spatial isolation of active sites promoting catalysis†

Kai Zhang, Xingyun Cao, Zhiyan Zhang, Yong Cheng and Ying-Hua Zhou *

Development of an efficient catalyst for degradation of organophosphorus toxicants is highly desirable. Herein, an MIL-101(Cr) LZn catalyst was fabricated by incorporating polypyridine zinc complexes into a MOF to achieve the spatial isolation of active sites. Compared with a terpyridine zinc complex without an MIL-101 support, this catalyst was highly active for detoxification of diethyl-4-nitrophenylphosphate.

Organophosphate-containing nerve agents can severely inhibit the activity of acetylcholinesterase which is involved in the transmission of neural signals, and thus are a potential hazard to mankind and the environment.[1–3] Although production and use of chemical warfare agents are prohibited by international treaty, still there is a risk of stockpile leakage and abuse of highly toxic organophosphorus (OP) compounds such as sarin, tabun, and VX.[4,5] Therefore, design and fabrication of efficient catalytic materials for OP detoxification are highly desirable. In this regard, OP destruction generally involves hydrolysis *via* an S_N2 nucleophilic attack on a phosphorus atom,[6] and OP degradation can also proceed through oxidation by light irradiation.[7] Currently, photocatalysts for OP oxidation cannot meet practical requirements, due to the intrinsic recombination between the photoinduced electrons and holes.[8] To this end, a number of catalytic materials have been developed for OP hydrolysis by the cleavage of the P–O bond. These materials include metal hydrolase (phosphotriesterase), a homogeneous catalyst (metal complex) and a heterogeneous catalyst (metal oxide and coordination polymer).[9–12] It is well known that enzymes are usually utilized only under physiological conditions. Regardless of the outstanding activity in OP hydrolysis, the metal complexes as homogeneous catalysts are responsible for dimerization in basic solution, thus resulting in deactivation.[13,14] Heterogeneous catalysts with spatially isolated active sites can lessen or avoid the above tendency of inactivation.[15] Therefore, it is highly desirable to incorporate functional complexes into the heterogeneous materials to gain efficient hydrolysis of OP toxicants.

On the other hand, metal–organic frameworks (MOFs) are regarded as an important class of porous crystalline materials by virtue of their distinctive attributes, such as their well-defined structure, high surface area, tunable pore aperture, and tailorable composition.[16–18] The porous channels in MOFs are favorable for the diffusion of the substrate and products, and the metal centers arranged in nodes and/or building blocks of MOFs can serve as active sites for the catalysis.[19–22] The highly stable Zr(IV)-based MOFs can be directly used to catalyse the degradation of the OPs and their simulants, with the merits of the strong Lewis acidity originating from the metal clusters at the MOF nodes.[23–25] Chromium-based MOFs modified with dialkylaminopyridines exhibited synergistic catalysis during OP hydrolysis, wherein Cr^{3+} ions acted as a Lewis acid to polarize the P–O bond and the implanted amino-containing groups served as a Lewis base for the nucleophilic attack toward the phosphorus atom.[26] The mesoporous MIL-101(Cr) ($Cr_3F(H_2O)_2O(TPA)_3{\cdot}nH_2O$, TPA = terephthalic acid) was deemed to be the perfect scaffold for the supported catalyst,[27,28] owing to the presence of two large inner cages, high Langmuir surface area, and high chemical stability. Furthermore, MIL-101(Cr) can be easily functionalized, wherein the coordinated water molecules can be displaced with some appropriate auxiliary ligands.[29] Accordingly, MIL-101(Cr) might be expected to play a role as a promising platform of multi-site catalysts for OP detoxification. The main hypothesis of this work is that the catalytic activity of MIL-101(Cr) can be further enhanced by grafting functional complexes into the nodes of MOFs to create additional active sites for OP hydrolysis.

Herein, an MIL-101(Cr)LZn catalyst (L = 4′-(4-pyridyl)-2,2′:6′,2″-terpyridine) was fabricated by incorporating polypyri-

The Key Laboratory of Functional Molecular Solids, Ministry of Education, Anhui Laboratory of Molecule-Based Materials (State Key Laboratory Cultivation Base), College of Chemistry and Materials Science Anhui Normal University, Wuhu, Anhui 241002, P.R. China. E-mail: yhzhou@ahnu.edu.cn

†Electronic supplementary information (ESI) available. See DOI: 10.1039/d0dt04048g

dine zinc complexes into the metal clusters of MIL-101(Cr) by post-synthetic modification (PSM). The catalytic activity for the hydrolysis of diethyl-4-nitrophenylphosphate (DENP, paraoxon) as a nerve agent simulant was investigated. Moreover, ^{31}P NMR spectroscopy was applied to elucidate the cleavage pattern of phosphate ester in the process of hydrolysis.

As shown in Scheme 1, the MIL-101(Cr)LZn catalyst was prepared by incorporating polypyridine zinc complexes into the nodes of MIL-101(Cr) by the PSM method. It is well known that MIL-101(Cr) presents a structure consisting of a three-dimensional network containing two large cavities with diameters of *ca.* 29 and 34 Å, respectively, in which the μ_3-O-Cr_3 clusters are linked *via* benzene dicarboxylate.[27] It is noteworthy that each Cr^{3+} ion is ligated with a water molecule or hydroxyl group. Therefore, the coordination unsaturated sites of MIL-101(Cr) could be created by the removal of coordination water molecules in the nodes of MOFs. Then, the ditopic ligand of 4′-(4-pyridyl)-2,2′:6′,2″-terpyridine (PTP, L) in anhydrous toluene was added to promote the coordinative interaction between the pyridine moiety of PTP and the Cr cluster of MIL-101(Cr), resulting in the formation of MIL-101(Cr)L. Subsequently, zinc perchlorate was introduced to achieve the formation of MIL-101(Cr)LZn, in which each zinc ion was coordinated by three N atoms of the terpyridine group in the auxiliary ligand of PTP. The resultant MIL-101(Cr)LZn was identified using PXRD patterns (Fig. 1a). The peaks of MIL-101(Cr)LZn and as-synthesized MIL-101(Cr) are in a good accordance with the simulated PXRD pattern of the reported crystal structure,[29] indicative of no apparent loss of crystallinity and framework structure after PSM. Importantly, the integrity of the crystal framework structure was still retained when MIL-101(Cr)LZn was treated for 6 h in sodium hydroxide solution at pH 10.0, showing that this robust MOF derivative could act as an ideal catalytic platform for the hydrolytic reaction in favor of the basic conditions. Moreover, the Brunauer–Emmett–Teller (BET) surface area of the MOF derivative was evaluated by using its nitrogen adsorption and desorption isotherms at 77 K (Fig. 1b). The BET surface area of as-synthesized MIL-101(Cr) and MIL-101(Cr)LZn was 3238 and 1652 $m^2\ g^{-1}$, respectively. The significant reduction of surface area after PSM is attributed to the presence of functionalized groups. Compared to MIL-101(Cr), MIL-101(Cr)LZn presented a decrease in Barrett–Joyner–Halenda (BJH) pore volume (Fig. S1†). It can be ascribed to the incorporation of polypyridine zinc complexes into the nodes of MIL-101(Cr). Moreover, FT-IR spectra (Fig. S2†) were investigated. Compared to MIL-101(Cr), MIL-101(Cr)L presented new peaks at 1587, 883 and 833 cm^{-1}, which were assigned to the stretching vibrations of C=N in terpyridine, and the symmetrical and asymmetrical stretching vibrations of C–H in the pyridine group,[30] respectively. This demonstrates the successful incorporation of polypyridine ligands into MIL-101(Cr). Furthermore, the scanning electron microscopy (SEM) images revealed that MIL-101(Cr)LZn exhibited a well-defined octahedron-like morphology with the particles having an average size of ~300 nm (Fig. 1c–e), similar to the morphology of MIL-101(Cr) and MIL-101(Cr)L. This indicated that the robust MIL-101(Cr)LZn could maintain the crystal morphology of MIL-101. Transmission electron microscopy (TEM) images and the elemental mapping analysis of MIL-101(Cr)LZn are shown in Fig. 1f–k, which reveal

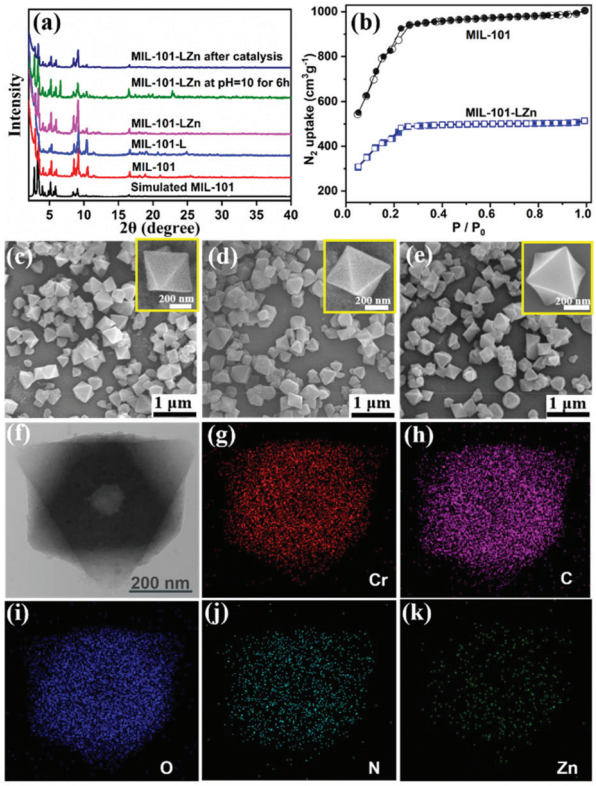

Fig. 1 (a) PXRD patterns of MIL-101(Cr), MIL-101(Cr)L, and MIL-101(Cr)LZn treated for 6 hours at pH = 10 and after the catalytic reaction of paraoxon hydrolysis. (b) N_2 adsorption and desorption isotherms of MIL-101(Cr) and MIL-101(Cr)LZn at 77 K. SEM images of (c) MIL-101(Cr), (d) MIL-101(Cr)L and (e) MIL-101(Cr)LZn; (f–k) TEM image and elemental mapping results of MIL-101(Cr)LZn.

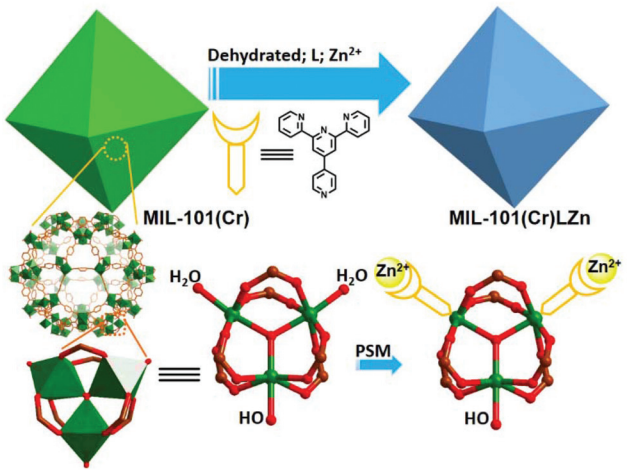

Scheme 1 Schematic diagram for the preparation of MIL-101(Cr)LZn.

uniform distribution of Cr, Zn, C, and O elements. By inductively coupled plasma mass spectrometry (ICP-MS), the Cr : Zn ratio of MIL-101(Cr)LZn was determined to be 1 : 0.14 (calcd: 1 : 0.67), where the functionalization yield is 21%. The value was slightly higher than the Cr/Zn atomic ratio (*ca.* 93 : 7) measured from the EDS spectrum (Fig. S3†), which might be attributed to the slight difference of zinc distribution between that on the surface and in the bulk. The thermogravimetric (TG) curves (Fig. S4†) demonstrated that the mass loss of MIL-101(Cr)L (~24 wt%) was observed in a temperature range of 50–350 °C, due to the removal of water and solvents, and this was lower than that of MIL-101(Cr). This indicated that some water molecules in MIL-101(Cr)L were displaced by PTP auxiliary ligands. The pyrolysis of the organic ligands and framework collapse in the MOFs occurred in a range of 350–500 °C, and finally generated chromium oxide.

The catalytic activity of MIL-101(Cr)LZn was evaluated by the hydrolytic degradation of ethyl-paraoxon (diethyl-4-nitrophenylphosphate, DENP), which is a simulant for an OP nerve agent. It was found that during the hydrolysis process of DENP (0.1 mM) in the presence of MIL-101(Cr)LZn (5.0 mg mL^{-1}) at pH 10 and 313 K, UV-vis absorption at 400 nm increased with the time extension (Fig. 2a), attributed to DENP decomposition to generate *p*-nitrophenolate.[7,31] The value of the *pseudo*-first order rate constant (k_{obs}) was determined from the initial slope in the plot of ln $[A_\infty/(A_\infty - A_t)]$ against time from 0 to 6 h (Fig. 2b). Comparative experiments of MIL-101(Cr) and its derivatives were also carried out (Fig. S5†). MIL-101(Cr) exhibited catalytic performance with a k_{obs} value of 0.118 h^{-1}, owing to the Lewis acidity of the Cr cluster in MIL-101(Cr).[32,33] Strangely, the catalytic performance of MIL-101(Cr)L reduced by about 50% in comparison with that of the activated MIL-101(Cr). This might account for the decrease of Lewis acidity in MIL-101(Cr) node, due to the coordination interaction between Cr ions and the additive ligands of PTP. It is noteworthy that the activity of the zinc terpyridine complex as a ZnL analogue was slight, with a k_{obs} value of 0.016 h^{-1}. This could be attributed to the fact that each zinc ion was ligated to six nitrogen atoms from two equivalents of the tridentate ligand 2,2′:6′,2″-terpyridine (L′), deduced from the PXRD pattern (Fig. S6†).[34] This complex presented saturated coordination, leading to the inert activity. Importantly, the reaction rate of MIL-101(Cr)LZn with a k_{obs} value of 0.154 h^{-1} almost exceeded two times that of MIL-101(Cr)L, attributed to the strong nucleophilicity of the implanted Zn complex in the buffer solution with pH 10.0.[35] The incorporated ligands L were well-arranged in the nodes of MIL-101(Cr), and thus the unsaturated-coordination sites of the ZnL complex were occupied by water molecules. After deprotonation of the coordinated water from the implanted complex $[ZnL(H_2O)_2](ClO_4)_2$ under the basic conditions,[14,36] the Zn-OH species as a Lewis base made a nucleophilic attack on the phosphorus atom of the DENP substrate. Therefore, MIL-101(Cr)LZn exhibited a synergistic effect between the Cr cluster as the Lewis acid and the zinc complex as the Lewis base for OP hydrolysis. MIL-101(Cr)LZn exhibited comparable catalytic activity to most of the heterogeneous and homogeneous catalysts for DENP degradation (Table 1).[26,37–39] Compared to MIL-101(Cr) and MIL-101(Cr)L, MIL-101(Cr)LZn exhibited the highest activity for the catalytic performance for DENP hydrolysis at pH 10.0 and 313 K (Fig. 2c). In the control experiments, self-hydrolysis of DENP was demonstrated to be negligible under the same conditions.

Moreover, DENP degradation catalyzed by MIL-101(Cr)LZn was performed under various basic conditions to explore the pH effect. It was found that in the presence of MIL-101(Cr)LZn, the reaction conversion at pH 7.0 was just 60% after 12 h (Fig. 2d). However, within 12 h, the corresponding k_{obs} values continuously increased with respect to the basicity of the buffer solution (Fig. S7†). The phenomenon distinctly differs from that of simple Zn complexes as homogeneous catalysts, which always suffer from deactivation induced by hydroxyl-

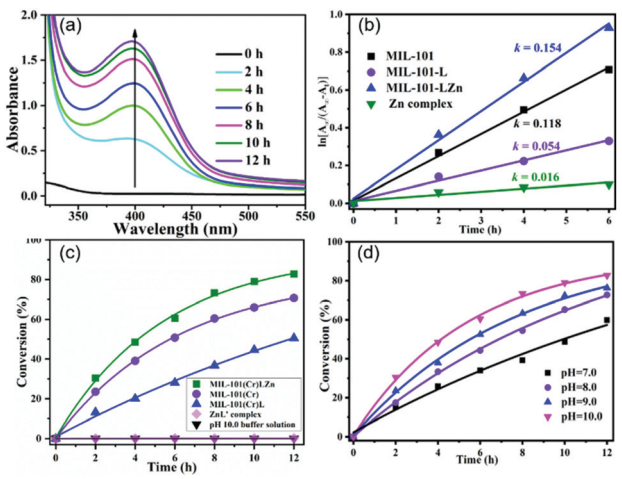

Fig. 2 (a) UV-vis absorption vs time for DENP hydrolysis at pH 10 over MIL-101(Cr)LZn; (b) Kinetic profiles of DENP hydrolysis catalyzed by MIL-101(Cr), MIL-101(Cr)L, MIL-101(Cr)LZn and 2,2′:6′,2″-terpyridine zinc complex. The plots of conversion vs time for DENP hydrolysis in the presence of (c) different catalysts at pH 10.0; and (d) MIL-101(Cr)LZn in the buffer solution of different pH values. Conditions: 5.0 mg mL^{-1} catalyst, 0.1 mM DENP and at 313 K.

Table 1 Rate constant of DENP hydrolysis in the presence of various catalysts

Catalyst amount	Conditions	k_{obs} (h^{-1})	Ref.
MIL-101(Cr)LZn[a] (5.0 mg L^{-1})	pH 10.0, 313 K	0.154	This work
MIL-101(Cr) (5.0 mg L^{-1})	pH 10.0, 313 K	0.118	This work
MIL-101-A[b] (4.8 mmol L^{-1})	pH 10.0, 298 K	0.140	26
$Zn_2(H_2L^3)_2(NO_3)_2$[c] (0.8 mmol L^{-1})	pH 8.5, 323 K	0.014	37
Zn^{2+}–[12]aneN$_3$[d] (1.36 mmol L^{-1})	pH 8.1, 323 K	0.036[e]	38
Cp_2MoCl_2[f] (50 mmol L^{-1})	pH 3.0, 313 K	0.021[g]	39

[a] L = 4′-(4-pyridyl)-2,2′:6′,2″-terpyridine. [b] A = 4-dimethylaminopyridine. [c] H_3L^3 = (*E*,*E*)-(4-methyl-1*H*-pyrazole-3,5-diyl)bis(methylmethanone) dioxime. [d] [12]aneN$_3$ = η^5-$C_5H_5$1,5,9-triazacyclododecane. [e] 6.08×10^{-4} min^{-1}. [f] Cp = η^5-C_5H_5. [g] 5.7×10^{-6} s^{-1}.

bridged dimerization in basic solutions.[14,40] It can be explained that the spatial isolation of the Zn complex in the node of MOFs is beneficial for the prevention of the formation of a Zn-μ_2-(OH)-Zn complex and thus perfect activity is observed. Additionally, the catalytic performance of MIL-101 (Cr)LZn increased as a function of temperature (Fig. 3a). Thus, the activation energy (E_a), obtained by the fitting of Arrhenius law, was found to be 25.56 kJ mol^{-1} (Fig. S8†), lower than those of most of the reported catalysts,[41] indicating a suitable transition state with a narrow activation barrier during this catalysis.

To explore the effect of MOF size on the catalytic activity, the small-sized MIL-101LZn (denoted as s-MIL-101(Cr)LZn) with a size of ~150 nm was prepared through the PSM of s-MIL-101(Fig. S9†). Compared with MIL-101(Cr)LZn (Fig. S10†), s-MIL-101(Cr)LZn exhibited lower activity for DENP degradation under the same conditions. Moreover, the stability of s-MIL-101(Cr)LZn was poor, confirmed by the XRD pattern of the sample after catalysis (Fig. S11†). This might be attributed to the lower crystallization degree induced by the synthetic conditions of the MOF (433 K and DMF/H_2O solvent for s-MIL-101(Cr) whereas 473 K and only H_2O solvent for MIL-101 (Cr)).[42] Since the porous MIL-101(Cr) with large cavities could be functionalized by the modification of the secondary building units, the functional groups both on the outer surface and inside the pores of MIL-101(Cr) derivatives would play vital roles in the catalysis.[43,44]

To further investigate the reaction mechanism, the spectra of ^{31}P NMR had been studied. It was found that when the reaction proceeded for an hour, a strong peak appeared at −6.54 ppm (Fig. 3b), identified as the substrate of DENP, and a weak peak was observed at 0.75 ppm, assigned to diethyl phosphate. The disappearance of the peak at −6.54 ppm and only the presence of the peak at 0.75 ppm could be found after the complete hydrolysis of DENP. Therefore, as shown in Scheme 2, the cleavage of the P–O bond occurred and it generated the products including diethyl phosphate and *p*-nitrophenolate during DENP degradation catalyzed by MIL-101(Cr)LZn.

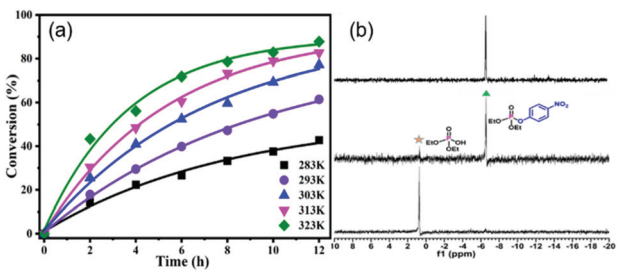

Fig. 3 (a) Kinetic profiles of the conversion vs time for DENP (0.1 mM) hydrolysis catalyzed by MIL-101(Cr)LZn (5.0 mg mL^{-1}) at pH 10.0 and different temperatures; (b) ^{31}P NMR spectra of DENP solution (the upper line) catalyzed by MIL-101(Cr)LZn for 1.0 h (the middle line) and 2 d (the bottom line) at pH 10.0 and 313 K. Diethylphosphoric acid (δ 0.75) and DENP (δ −6.54).

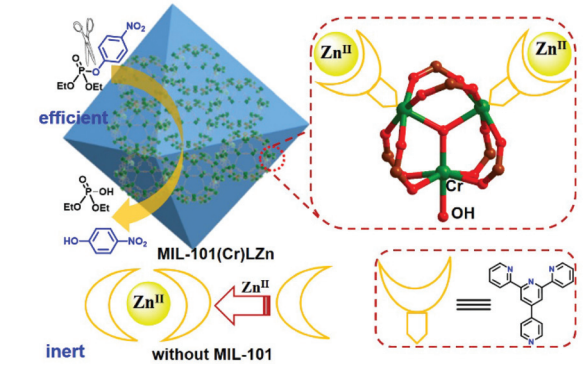

Scheme 2 The proposed illustration of DENP hydrolysis catalyzed by MIL-101(Cr)LZn.

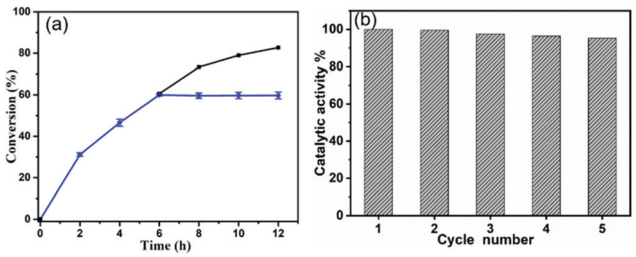

Fig. 4 (a) Kinetic profiles of the conversion *versus* time for DENP (0.1 mM) hydrolysis catalyzed by MIL-101(Cr)LZn (5.0 mg mL^{-1}) with removal of the catalyst at pH 10 and 313 K after 6 h; (b) cycling test of DENP hydrolysis catalyzed by MIL-101(Cr)LZn at pH 10 and 313 K, in which the activity was evaluated from the conversion ratio after 12 h. The activity in the first run was denoted as 100%.

To investigate the stability of the heterogeneous catalyst, MIL-101-LZn was removed from the reaction system by centrifugation after 6 h. As a result, no noticeable increment of the conversion of DENP was observed (Fig. 4a), indicating that the active component of the Zn complex and Cr cluster did not leach out.[45] Therefore, the MIL-101(Cr)LZn catalyst maintained the significant stability. Moreover, the reusability of the MIL-101(Cr)LZn catalyst was surveyed. It was found that the catalytic activity of MIL-101(Cr)LZn could be retained at 96% in the fifth run for DENP hydrolysis (Fig. 4b). Furthermore, the framework structure of MIL-101(Cr)LZn showed no significant change after the catalysis, as determined from the XRD pattern (Fig. 1a). The abovementioned experiments demonstrated the great recyclability and good stability of MIL-101(Cr)LZn toward the hydrolysis of OPs.

Conclusions

The catalyst MIL-101(Cr)LZn has been designed and fabricated by incorporating poly-pyridine zinc complexes through the post-synthetic modification of MOFs. This heterogeneous catalyst exhibited significant performance for the catalytic degradation of simulated highly toxic nerve agents such as

diethyl-4-nitrophenylphosphate. The remarkable catalytic activity can be ascribed to the implanted functional zinc complexes as Lewis base sites and Cr clusters as Lewis acid sites. The perfect stability of this catalyst is attributed to the inherited properties of MIL-101(Cr), and the unique spatially isolated zinc complexes at the nodes of the MOF. We anticipate that this study will pave a new avenue toward designing MOF-based multifunctional catalysts for a variety of chemical transformations and hydrolysis of nerve agents in real-world applications.

Conflicts of interest

There are no conflicts to declare.

Acknowledgements

This work was supported by the National Natural Science Foundation of China (Grant No. 21771004).

Notes and references

1 G. Mercey, T. Verdelet, J. Renou, M. Kliachyna, R. Baati, F. Nachon, L. Jean and P. Y. Renard, *Acc. Chem. Res.*, 2012, **45**, 756–766.
2 M. B. Colovic, D. Z. Krstic, T. D. Lazarevic-Pasti, A. M. Bondzic and V. M. Vasic, *Curr. Neuropharmacol.*, 2013, **11**, 315–335.
3 L. Gorecki, O. Gerlits, X. T. Kong, X. L. Cheng, D. K. Blumenthal, P. Taylor, C. Ballatore, A. Kovalevsky and Z. Radic, *J. Biol. Chem.*, 2020, **295**, 4079–4092.
4 S. Vucinic, B. Antonijevic, A. M. Tsatsakis, L. Vassilopoulou, A. O. Docea, A. E. Nosyrev, B. N. Izotov, H. Thiermann, N. Drakoulis and D. Brkic, *Environ. Toxicol. Pharmacol.*, 2017, **56**, 163–171.
5 K. K. Ma, T. Islamoglu, Z. J. Chen, P. Li, M. C. Wasson, Y. W. Chen, Y. F. Wang, G. W. Peterson, J. H. Xin and O. K. Farha, *J. Am. Chem. Soc.*, 2019, **141**, 15626–15633.
6 A. Zammataro, R. Santonocito, A. Pappalardo and G. T. Sfrazzetto, *Catalysts*, 2020, **10**, 881–898.
7 T. Khedr, A. A. Hammad, A. M. Elmarsafy, E. Halawa and M. Soliman, *J. Hazard. Mater.*, 2019, **373**, 23–28.
8 S. Garcia-Segura and E. Brillas, *J. Photochem. Photobiol., C*, 2017, **31**, 1–35.
9 H. B. Li, L. Ma, L. Y. Zhou, J. Gao, Z. H. Huang, Y. He and Y. J. Jiang, *Chem. Commun.*, 2018, **54**, 10754–10757.
10 B. M. Smith, *Chem. Soc. Rev.*, 2008, **37**, 470–478.
11 T. Islamoglu, Z. Chen, M. C. Wasson, C. T. Buru, K. O. Kirlikovali, U. Afrin, M. R. Mian and O. K. Farha, *Chem. Rev.*, 2020, **120**, 8130–8160.
12 J. A. Harvey, C. J. Pearce, M. G. Hall, E. J. Bruni, J. B. DeCoste and D. F. S. Gallis, *Dalton Trans.*, 2019, **48**, 16153–16157.
13 Y. H. Zhou, L. Q. Chen, J. Tao, J. L. Shen, D. Y. Gong, R. R. Yun and Y. Cheng, *J. Inorg. Biochem.*, 2016, **163**, 176–184.
14 A. K. Yatsimirsky, *Coord. Chem. Rev.*, 2005, **249**, 1997–2011.
15 R. Ye, J. Zhao, B. B. Wickemeyer, F. D. Toste and G. A. Somorjai, *Nat. Catal.*, 2018, **1**, 318–325.
16 M. L. Ding, X. C. Cai and H. L. Jiang, *Chem. Sci.*, 2019, **10**, 10209–10230.
17 H. Furukawa, K. E. Cordova, M. O'Keeffe and O. M. Yaghi, *Science*, 2013, **341**, 1230444.
18 Y. Bai, Y. B. Dou, L. H. Xie, W. Rutledge, J. R. Li and H. C. Zhou, *Chem. Soc. Rev.*, 2016, **45**, 2327–2367.
19 Q. Liu, H. J. Cong and H. X. Deng, *J. Am. Chem. Soc.*, 2016, **138**, 13822–13825.
20 Y. S. Kang, Y. Lu, K. Chen, Y. Zhao, P. Wang and W. Y. Sun, *Coord. Chem. Rev.*, 2019, **378**, 262–280.
21 D. D. Li, M. Kassymova, X. C. Cai, S. Q. Zang and H. L. Jiang, *Coord. Chem. Rev.*, 2020, **412**, 213262.
22 K. Vellingiri, L. Philip and K.-H. Kim, *Coord. Chem. Rev.*, 2017, **353**, 159–179.
23 Y. Y. Liu, A. J. Howarth, N. A. Vermeulen, S. Y. Moon, J. T. Hupp and O. K. Farha, *Coord. Chem. Rev.*, 2017, **346**, 101–111.
24 M. C. de Koning, M. van Grol and T. Breijaert, *Inorg. Chem.*, 2017, **56**, 11804–11809.
25 A. M. Plonka, Q. Wang, W. O. Gordon, A. Balboa, D. Troya, W. W. Guo, C. H. Sharp, S. D. Senanayake, J. R. Morris, C. L. Hill and A. I. Frenkel, *J. Am. Chem. Soc.*, 2017, **139**, 599–602.
26 S. Wang, L. Bromberg, H. Schreuder-Gibson and T. A. Hatton, *ACS Appl. Mater. Interfaces*, 2013, **5**, 1269–1278.
27 G. Férey, C. Mellot-Draznieks, C. Serre, F. Millange, J. Dutour, S. Surblé and I. Margiolaki, *Science*, 2005, **309**, 2040–2042.
28 A. Celeste, A. Paolone, J.-P. Itié, F. Borondics, B. Joseph, O. Grad, G. Blanita, C. Zlotea and F. Capitani, *J. Am. Chem. Soc.*, 2020, **142**, 15012–15019.
29 D. Y. Hong, Y. K. Hwang, C. Serre, G. Férey and J. S. Chang, *Adv. Funct. Mater.*, 2009, **19**, 1537–1552.
30 N. M. Logacheva, V. E. Baulin, A. Y. Tsivadze, E. N. Pyatova, I. S. Ivanova, Y. A. Velikodny and V. V. Chernyshev, *Dalton Trans.*, 2009, 2482–2489.
31 X. J. Ma, L. Zhang, M. F. Xia, S. Q. Li, X. H. Zhang and Y. D. Zhang, *ACS Appl. Mater. Interfaces*, 2017, **9**, 21089–21093.
32 F. Yang, C.-X. Yang and X.-P. Yan, *Talanta*, 2015, **137**, 136–142.
33 B. Li, D. Ma, Y. Li, Y. Zhang, G. Li, Z. Shi, S. Feng, M. J. Zaworotko and S. Ma, *Chem. Mater.*, 2016, **28**, 4781–4786.
34 I. Šloufová, B. Vlčková, P. Mojzeš, I. Matulková, I. Císařová, M. Procházka and J. Vohlídal, *J. Phys. Chem. C*, 2018, **122**, 6066–6077.
35 D. Desbouis, I. P. Troitsky, M. J. Belousoff, L. Spiccia and B. Graham, *Coord. Chem. Rev.*, 2012, **256**, 897–937.

36 Y. H. Zhou, H. Fu, W. X. Zhao, M. L. Tong, C. Y. Su, H. Sun, L. N. Ji and Z. W. Mao, *Chem. – Eur. J.*, 2007, **13**, 2402–2409.
37 L. V. Penkova, A. Maciąg, E. V. Rybak-Akimova, M. Haukka, V. A. Pavlenko, T. S. Iskenderov, H. Kozłowski, F. Meyer and I. O. Fritsky, *Inorg. Chem.*, 2009, **48**, 6960–6971.
38 D. J. Kennedy, B. P. Mayer, S. E. Baker and C. A. Valdez, *Inorg. Chim. Acta*, 2015, **436**, 123–131.
39 L. Y. Kuo and N. M. Perera, *Inorg. Chem.*, 2000, **39**, 2103–2106.
40 D. Prochowicz, K. Sokolowski and J. Lewinski, *Coord. Chem. Rev.*, 2014, **270**, 112–126.
41 M. Erdem, R. Say, A. Ersöz, A. Denizli and H. Türk, *React. Funct. Polym.*, 2010, **70**, 238–243.
42 B. Tan, Y. Luo, X. Liang, S. Wang, X. Gao, Z. Zhang and Y. Fang, *Ind. Eng. Chem. Res.*, 2019, **58**, 2983–2990.
43 Y. Hu, W. M. Verdegaal, S.-H. Yu and H.-L. Jiang, *ChemSusChem*, 2014, **7**, 734–737.
44 B. Li, Y. Zhang, D. Ma, L. Li, G. Li, G. Li, Z. Shi and S. Feng, *Chem. Commun.*, 2012, **48**, 6151–6153.
45 S. N. Ansari, P. Kumar, A. K. Gupta, P. Mathur and S. M. Mobin, *Inorg. Chem.*, 2019, **58**, 9723–9732.